Aerodynamic Study of Wingtip-mounted Propeller and Distributed Propulsion System

Geng Qiao
CFD Laboratory
School of Engineering,
University of Glasgow,
Scotland, UK

George N. Barakos
CFD Laboratory
School of Engineering,
University of Glasgow,
Scotland, UK

ABSTRACT

Today, most innovative vehicle designs, such as those with distributed propulsion (DP) systems, are equipped with multiple rotors and propellers. DP systems create complex interactional aerodynamics, which remain largely unexplored and not fully understood. This paper presents a high-fidelity aerodynamic analysis of a tip-mounted propeller (TMP) combined with an over-the-wing (OTW)-installed system. Four configurations were tested using fully resolved simulations with the HMB3 CFD solver. The results indicate that the interactional effects in all configurations influence the propeller and wing performance. Notably, the proposed configuration featuring both TMP and DP produced 3.5% more thrust compared to the configuration with TMP-only, while also enhancing efficiency. This improved wing performance, yielding more lift, less drag and resulted in higher lift-to-drag ratio (L/D). These benefits were due to the thrust distribution and propeller slipstream. Additionally, the OTW-DP system resulting in higher pitching moments, suggesting that the entire vehicle should be considered to achieve the overall objective of high efficiency.

NOTATION

*

Symbols

C_p Pressure coefficient, $C_p = \dfrac{p - p_\infty}{0.5\rho U_\infty^2}$

$C_{T\,prop}$ Propeller thrust coefficient, $C_{T\,prop} = \frac{T}{\rho n^2 D^4}$

$C_{Q prop}$ Propeller torque coefficient, $C_{Q prop} = \frac{Q}{\rho n^2 D^5}$

c Characteristic length, m

k Specific turbulent kinetic energy, $\mathrm{m^2 s^{-2}}$

ω Specific dissipation frequency of turbulence

M_∞ Mach number

n Rotational speed, Hz

Q Rotor torque $[N.m]$

N_b Number of blades

R Flow residual vector

T Thrust, N,kN

U Local velocity, m/s

U_∞ Free-stream velocity, m/s

W Conservative flow variables

η Froude efficiency, $\eta = \frac{TU_\infty}{Q\Omega}$

Ω Rotational velocity, rad/s

i, j, k Block index

*

Acronyms

CFD Computational Fluid Dynamics

DP Distributed Propulsion

HMB Helicopter Multi-Block

HLP High Lift Propeller

NASA National Aeronautics and Space Administration

RPM Revolutions Per Minute

RANS Reynolds-Averaged Navier-Stokes

SAS Scale-Adaptive Simulation

SST Shear Stress Tensor

TP Tip-mounted Propeller

INTRODUCTION AND OBJECTIVES

Recent advancements in hybrid and electric propulsion technologies enable the development of distributed propulsion systems, which have the potential to reduce energy consumption and emissions (Ref. 1). An analysis of aero-propulsive synergistic effects in the preliminary design phase indicates improvements in overall robustness, capacity, and system efficiency (Ref. 2). Aero-propulsive coupling, in particular, offers an intriguing method for enhancing wing lift augmentation. To comply with regulations on required stall speed, current designs often feature wings that are larger than necessary for cruising. Local wing blowing can increase dynamic pressure using the propulsion system, thereby raising the loading of wing sections. This approach allows for a reduction in wing area while still achieving the required stall speed and better cruise performance (Ref. 3).

Research on propellers is justified due to their superior efficiency compared to other propulsion methods. The installation of propellers on the airframe can significantly influences the overall aircraft performance. Notably, wingtip-mounted propellers are a promising configuration for reducing induced drag through favorable interaction effects. This is particularly true when the propeller rotation is opposite to that of the wingtip vortex in a tractor configuration, as this setup can help mitigate the induced drag (Refs. 4–6). In a pusher layout, where the propeller counter-rotates relative to the wingtip vortex, the swirling flow induced by the wingtip can lead to reduced shaft power (Refs. 6–8). However, this configuration also has drawbacks, including the adverse effects of a highly loaded wingtip, the significant weight of the engine, inertia loads, and a large yawing moment arm during one-engine-out scenarios.

Integrating wingtip-mounted propellers with a distributed propulsion system can enhance efficiency without compromising structural integrity or safety. Notable examples include the X-57 Maxwell aircraft (Ref. 9) and the Scalable Convergent Electric Propulsion Technology and Operations Research (SCEPTOR) concept (Ref. 10), which have attracted significant attention from industry, academia, and government. A detailed characterization of propeller-wing interaction effects is essential for developing novel flying vehicles. The Wingtip-mounted Propeller Workshop (WIPP), led by NASA, has provided valuable insights into tip-mounted propeller configurations through extensive experimental campaigns (Ref. 11). Prior research on distributed propulsion systems has optimized high-lift propeller installation locations using variable fidelity methods, demonstrating superior overall performance compared to conventional configurations from distributed propulsion system with the OTW design (Ref. 12). However, high-fidelity research combining tip-mounted propellers with distributed propulsion systems is currently rare. As a result, the performance and flow characteristics resulting from increased propeller-wing and propeller-propeller interactions remain largely unexplored.

This work employs a rigorously validated high-fidelity method, specifically designed to analyse propeller-wing and propeller-propeller interactions. For instance, this work examines configurations with tip-mounted propellers and distributed propulsion systems. Current work is aiming to identify the potential benefits of different emerging propulsion systems with a better understanding of the fundamental flow physics associated with each design.

NUMERICAL METHODS

The in-house Helicopter Multi-Block (HMB3) CFD solver is employed in this study. HMB3 can predict the aerodynamic performance and acoustics of propulsion systems, as shown in previous studies (Refs. 13, 14). HMB3 has been widely used in the investigation of rotorcraft flows (Refs. 15–18), helicopter rotor aeroelasticity (Ref. 19), propeller aeroacoustics (Ref. 20), flight mechanics (Ref. 21) and missile trajectory prediction (Ref. 22). Moreover, good agreement when compared to experimental results in aerodynamics, acoustics, and aeroelasticity of propellers has been reported in previous studies (Refs. 23–26). Most recently, its ability to capture the interactions of multi-rotor flows and estimate the performance of ducted propellers was also documented (Refs. 27–29).

HMB3 solves the Unsteady Reynolds Averaged Navier-Stokes (URANS) equation in integral form using the Arbitrary Lagrangian-Eulerian formulation for time-dependent domains, including moving boundary layers. HMB3 uses a cell-centered finite volume approach to discretise the Navier-Stokes equations on multi-block, structured grids.

$$\frac{d}{dt}\left(\mathbf{W}_{i,j,k}V_{i,j,k}\right) = -\mathbf{R}_{i,j,k}\left(\mathbf{W}_{i,j,k}\right), \qquad (1)$$

In Equation (1), i,j,k represent the cell index, $\mathbf{W}$ and $\mathbf{R}$ are the vector of conservative flow variables and the residual respectively, and $V_{i,j,k}$ is the volume of the cell i,j,k. The convective fluxes are evaluated using Osher's approximate Riemann solver, while the viscous terms are discretised using a second-order central differences scheme. The third-order MUSCL (Monotone Upstream-centered Schemes for Conservation Laws) approach provides high-order accuracy in space. In the present work, simulations are conducted using the $k-\omega$ shear stress transport (SST) turbulence model (Ref. 30) as this has been well-validated in previous studies of interactional aerodynamics (Refs. 31, 32).

For an isolated rotor in axial flight, the azimuthal symmetry of the configuration can be exploited, whereby only a fraction of the grid needs to be generated. The Rotating Reference Frame (RRF) method is implemented in HMB3 (Ref. 33) for simulations with rotational periodicity. The governing flow equations are solved in a non-inertial reference frame, thus transforming the unsteady problem into a steady one. For unsteady simulations, the entire grid is required. However, this can be obtained by copying and rotating the grids of the steady simulations using the HMB3 tools. Additionally, unsteady calculations are possible using the implicit, dual-time stepping approach. The computational grids used for rotor surfaces have a typical C-C topology. The spacing distribution has been set to the condition $\Delta y^+ < 1$, resulting in a first cell size of approximately $2.0 \times 10^{-6}c$ for all tested grids. Adiabatic wall boundary conditions are applied at rotors, with freestream values of pressure and velocity used elsewhere. Chimera overset grids are employed to capture the high-pressure gradient region and have been carefully designed for efficient load balancing. For the time-marching computations, a time step corresponding to two degrees of rotor rotation was used for all cases. The convergence of the implicit scheme was determined based on the reduction of the flow field residual compared to the previous time step. In particular, either a three-order-of-magnitude reduction or 300 inner iterations were considered sufficient for each unsteady step.

Furthermore, to assess the interference between propellers and lifting surfaces, it is evident that both components of each configuration cannot be independently evaluated. Thus, an integration of relevant forces (Thrust T, drag D) should be employed to comprehensively compare the overall performance of different configurations.

In Equation (2), the overall installed thrust (T_{install}) is calculated by subtracting the drag ($D_{\text{lifting surface}}$) of the lifting surface from the total thrust ($T_{\text{propellers}}$) generated by the propellers.

$$T_{install} = T_{propellers} - D_{liftingsurface} \tag{2}$$

Subsequently, the overall propulsive efficiency can be simplified, This can be seen in Equation (3). Here, V_∞ represents the free-stream velocity, and P_{shaft} denotes the power required by the propellers.

$$Overall\ propulsive\ efficiency\ (\eta) = \frac{T_{install} \times V_\infty}{P_{shaft}} \tag{3}$$

Finally, this study will apply the aforementioned equations to evaluate the overall performance of equivalent tractor and OTW distributed propulsion systems, where ensuring that the lifting surface is trimmed to produce the same amount of lift.

CFD VALIDATION

Given the tests conducted by Litherland et al. (Ref. 34) at the NASA Langley Research Centre at the Low-Speed Aeroacoustic Wind Tunnel, the current work aims to include the study of distributed propulsion systems based on previous numerical studies for the conformal folding High Lift Propeller (HLP) (Ref. 12). The HLP features five blades with a radius of 0.288 m and a fixed pitch of 24.1° at 75% of the blade radius. Various advance ratios, rotationa, and flight speeds were tested. The geometry details and a schematic of the propeller can be seen in (Ref. 32). The HMB3 CFD solver was employed to predict the performance, as illustrated in Figure 1 (a). Aerodynamic coefficients were compared against experiments at various advance ratios, showing good agreement between the results obtained from HMB3 and the experiments conducted by Litherland et al. (Ref. 34).

In an effort to bridge the knowledge gap in propeller/wing interactions, tests on wingtip-mounted propellers (WIPP) were conducted in the Lockheed Martin low-speed wind tunnel (LSWT) (Ref. 11). The test model of the WIPP featured a semi-span wing measuring 1.7 meters (67 inches) and a wingtip-mounted C-130 propeller scaled at 10% of the actual size. Measurements of forces and moments were collected at various angles of attack and thrust settings. The selected test cases were referenced as Cases 79 and 180 in the experimental report (Ref. 35), and the representative flow visualisation and comparisons are presented in Figure 1 (b)(c), with the results obtained using HMB3 showing good agreement with the experimental measurements.

DISTRIBUTED PROPULSION

With the CFD method validated, the investigation of the distributed propulsion system was conducted using the Workshop for Integrated Propeller Prediction (WIPP) geometry and the HLP. The flow visulisation of the OTWDP propulsion system is presented in Figure 2(b), and the performance of OTW propulsion system with different number of propellers installed is shown in Figures 2(a)(b). When transitioning from a single-propeller to a three-propeller Distributed Propulsion (DP) system, it was observed that the propellers became 14.2% more efficient. In terms of overall efficiency, the three-propeller Over-The-Wing (OTW) configuration was 26.3% more efficient than the single-propeller installed OTW configuration, demonstrating the capability of a DP system to enhance the overall performance.

TIP-MOUNTED PROPELLER AND DISTRIBUTED PROPULSION

A previous study (Ref. 12) on distributed propulsion systems found that the over-the-wing configuration, with varying numbers of installed HLPs, outperformed the tractor configurations in terms of overall performance. Additionally, research on tandem propellers (Ref. 36) has shown that both the tip-to-tip distance and downstream spacing significantly impact the performance and noise emissions due to their extensive interactions. Therefore, before conducting a comprehensive vehicle-level investigation, it is essential to examine the installation effects of tip-mounted and distributed propellers.

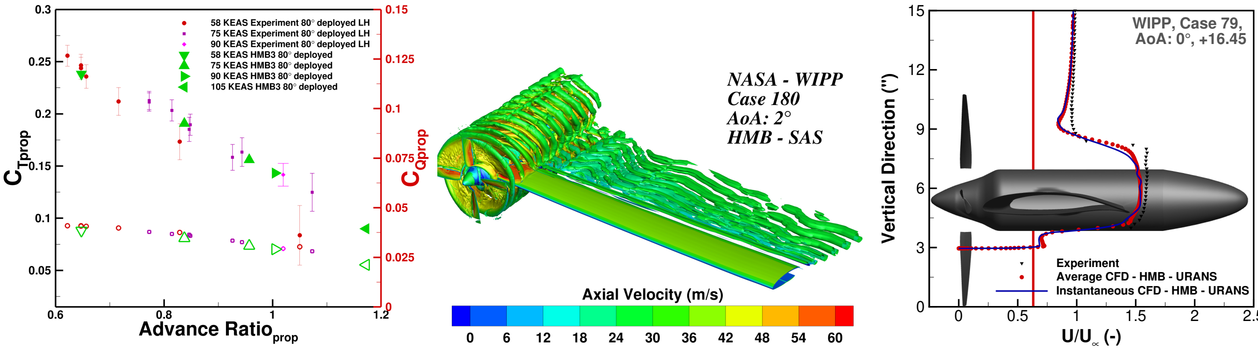

(a) High lift propeller. (b) Wingtip-mounted propeller (c) Wake 16.45.

Figure 1. (a) Validation of the HMB3 solver for HLP. (Ref. 34) (Ref. 32) Symbols filled with no colour represent the respective torque coefficients. (b) Flow visualisation of wingtip-mounted propeller. (c) Wake validation. (Refs. 31, 32)

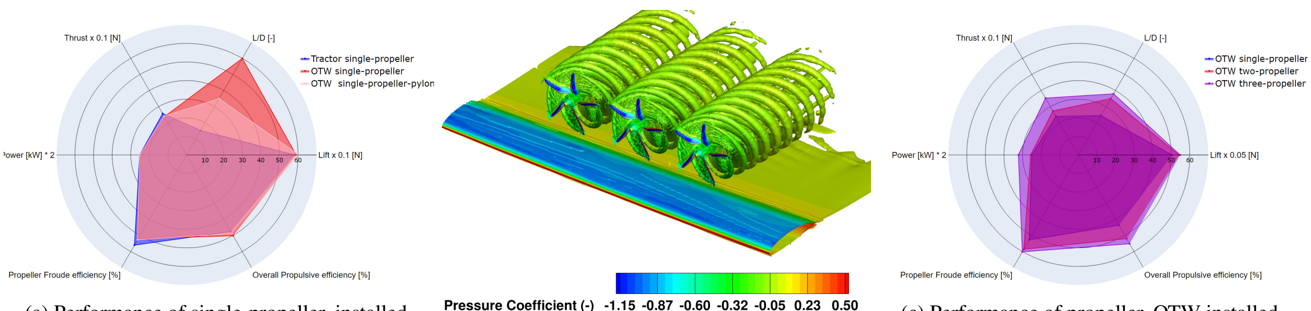

(a) Performance of single-propeller, installed, propulsion systems at RPM=4800. (b) Flow visualisation OTWDP system at μ =0.42. (c) Performance of propeller, OTW installed, propulsion systems.

Figure 2. Comparisons of the OTW configurations with single, two- and three-propeller, installed propulsion systems.

(a) C1 (b) C2

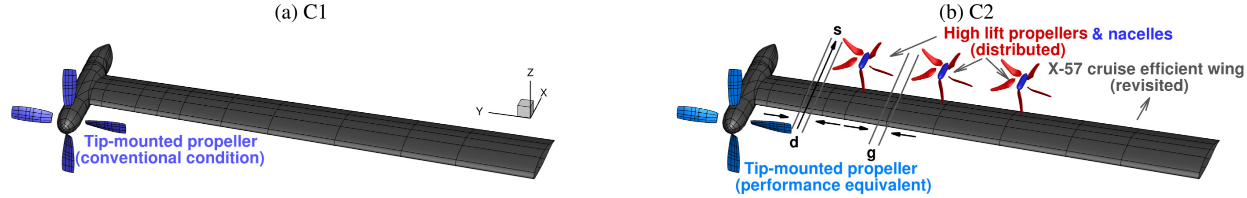

(c) C3 (d) C4

Figure 3. Schematic of investigated propeller installations.

Figure 3 shows four configurations. Configurations C1 and C4 are compared under identical operating conditions to isolate the aerodynamic interactions introduced by the DP system. The installed HLPs in configuration C2 are contrasted with the distributed HLPs in configuration C4 to assess the impact of TMP and the distribution of OTW-installed propellers. Furthermore, a comparative analysis is conducted between the TMP-only configuration, shown in Figure 3(c), and the TMPDP system, illustrated in Figure 3(d).

To maintain consistent flow physics, both scaled and full-scale, the same tip speed, corresponding to a Mach number of 0.505, is applied to the TMP in configuration C3, as used in the NASA WIPP experiment. In the TMPDP system of Figure 3(d), the RPM and collective pitch angle at 0.75R° are precisely adjusted to produce the same thrust as the propulsion system in Figure 3(c). Specifically, the TMP in configuration C4 operates at an RPM of 1850 with a collective pitch of 28°, while the DP operates at an RPM of 3700 with a collective pitch of 24.1°. This setup results in tip speeds of 0.286 for the TMP and 0.325 for the DP. The propeller spacing in configuration 3(d) is carefully designed to minimize performance losses due to aerodynamic interactions. Detailed specifications for all configurations are provided in Table 1.

The interactions of the wake structures of the four configu-

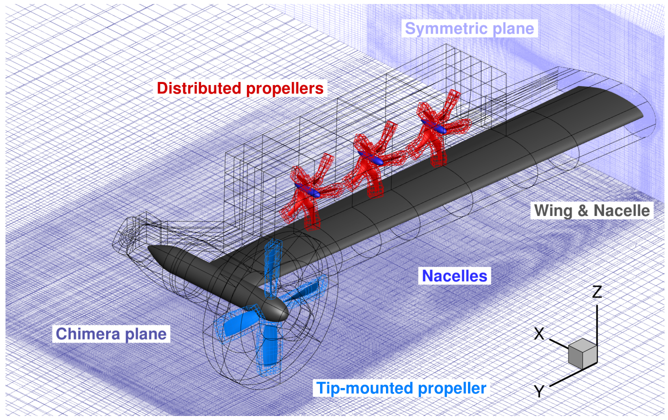

Figure 4. CFD grid topology used for TMPDP configuration.

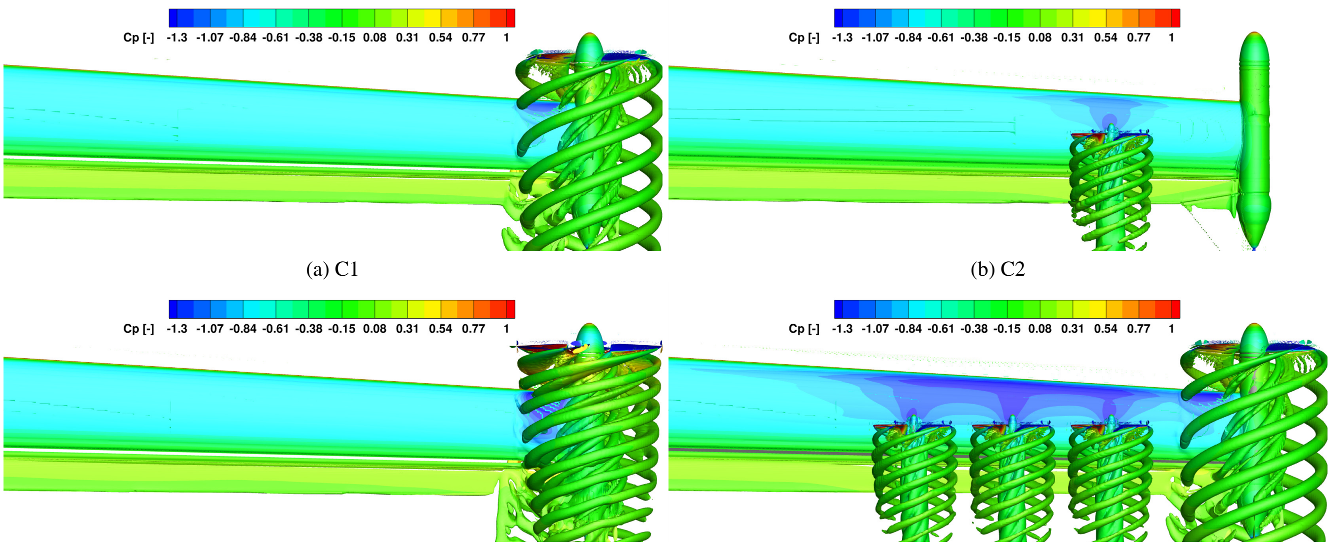

(a) C1 (b) C2 (c) C3 (d) C4

Figure 5. Flow visuilisation for varies configurations.

rations are presented using iso-surfaces of instantaneous Q-criterion, in Figure 5. In C1, the blade tip vortex, trailing edge vortex, root vortex, nacelle vortex, and wing trailing edge vortex are all observed. The tip vortex shows a relatively stable spiral structures and moves downstream along a helicoil path.

In the C2 configuration, a single OTW installed HLP shows more intense spiral structures due to its operation at higher RPM. The nacelle and blade root vortices show a cylindrical shape with spirals moving downstream and are more persistent than the tip vortices. The blade root and mid-span trailing edge vortices are mainly due to the non-uniform distribution of circulation on the propeller surface.

Moving to the C3 configuration, where the TMP is operating at a higher RPM at a tip Mach number of 0.505, the most intense spirals are observed following a helicoil path. Similar to the wing trailing edge around the spirals, a much stronger vortex sheet is formed due to the interactions with the spirals from TMP. This mutual distortion leads to the vortices deteriorating faster and shrinking.

When the TMP-DP system is simulated, the tip vortex structure is relatively similar to the C1 and C2 configurations since the configuration has been designed for minimal interactions from the different propellers.

Figure 6(a) illustrates the variation in single blade thrust over the full azimuth, scaled according to the tip-mounted propeller. The data reveal a performance drop in the tip-mounted propeller-only configurations, specifically in C1 and C3. This reduction in performance occurs as the blade passes near the wing. From configuration C1 to C3, both the severity of the performance loss and the extent of the affected region increase. This trend is due to the higher tip velocity in configuration C3, which introduces greater unsteady loads resulting from the interaction between the propeller and the wing.

Comparing the single-installed HLP with the distributed HLP, as represented by configurations C2 and C4, the setup involving distributed propellers demonstrates limited performance degradation due to the multi-propeller system. This is particularly evident with the second and third propellers, which are positioned sufficiently far from the TMP downwash. Notably, two peaks in performance are observed, corresponding to the

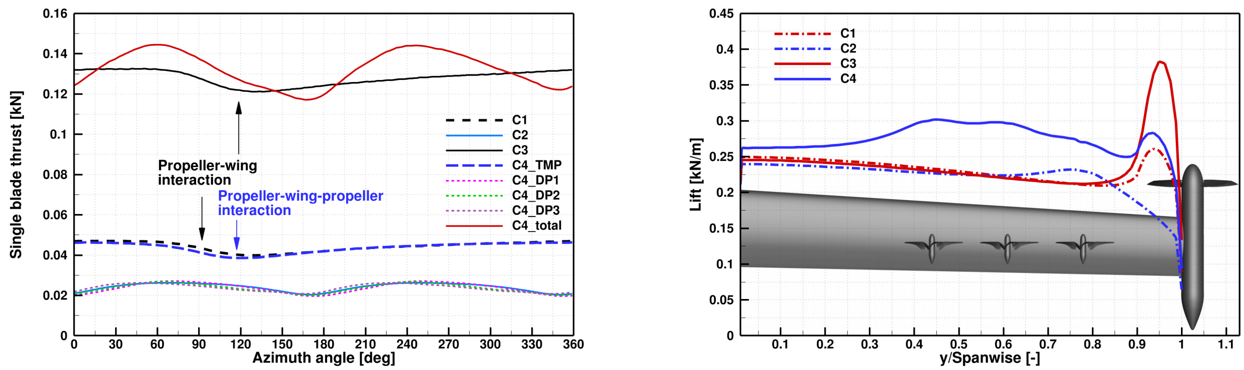

(a) Single blade thrust

(b) Lift distributionis

Figure 6. Single blade thrust variations and time-averaged lift distributionis from all configurations.

Table 1. Summary of the test condition used for the study of TMP and DP installed propulsion system.

Condition	Take-off and landing ($Ma_\infty = 0.08$)
Radius	
TMP	0.508 m
DP	0.288 m
RPM (Collective at 0.75R)	
TMP	3264 (19.5°), 1850 (28°) rev/min
DP	3700 (24.1°) rev/min
Blade tip Mach number	
TMP	0.505,0.286 -
DP	0.325 -
Configuration :	
Wing	-
Wing & TMP	Topout
Wing & TMP & DP	Topout
Tip-to-Tip Distance (d)	0.2 D_{TMP}
Downstream Spacing (s)	1.1 D_{TMP}
Tip-to-Tip Distance (g)	0.2 D_{DP}

distributed HLPs operating at twice the RPM of the TMP due to their smaller radius. Additionally, placing the distributed propeller $1.1D_{TMP}$ behind the TMP, with a tip-to-tip distance of $0.2D_{TMP}$, is effective in mitigating significant performance losses from installation effects. Furthermore, when examining the cumulative thrust loads from the C4 configuration, the overall thrust performance is enhanced, with the two peaks preserved, thanks to the additional thrust contribution from the distributed propellers.

Examining the averaged surface pressure coefficient across different configurations, as depicted in Figure 7, reveals that configurations C1 and C2 exhibit slightly lower suction pressures compared to C3 and C4. This difference is attributed to the single installed propeller operating at lower RPMs in C1 and C2. In contrast, configuration C3 shows the highest suction pressure among all configurations, particularly when compared to C1. This result indicates that a larger and more intense suction region is formed behind the TMP due to higher induced velocities. Consequently, the TMP in C3 significantly enhances lift generation from the wing.

In the C4 configuration, which includes both TMP and DP systems, a suction area similar to that in C1 is observed, as the TMP operates at the same RPM. However, there are minor effects from the DP installation in the region behind the TMP. Compared to C2, the DP system in C4 exhibit an expanded suction region, highlighting the favourable cooperative effect of the DP system. Within the DP system, the most significant suction region appears around the middle propeller, benefiting from the slipstream generated by the adjacent propellers. The interaction between the TMP and DP systems also results in favourable aerodynamic effects, as indicated by the suction profile in the TMP-DP system.

The effect of the pressure coefficient on the wing from different configurations alters the lift distribution along the wing span, as illustrated in Figure 6(b). In the C3 configuration, a sharp peak in lift distribution is observed behind the tip region of the TMP, caused by higher induced velocities. In contrast, this peak is significantly diminished in the C1 configuration, due to the lower induced velocities. In C2, an increase in wing performance is evident, particularly with a spike in lift generation at the propeller installation point. The C4 configuration shows a marked improvement in lift generation, featuring a reduced spike behind the TMP and a more uniform lift distribution. This uniformity is attributed to the beneficial effects of the DP system, which enhance the aerodynamic performance across the wing.

The propellers in the DP system create a distinct flow environment that benefits the wing. This design results in a smooth, high-lift spike originating from the innermost propeller. Overall, the relatively smooth lift distribution observed in the C4 configuration, as compared to the C3 configuration, indicates a favorable wing lift distribution achieved by the TMP-DP system.

The visualization of the vorticities presented in Figure 8 here to understand the different interaction mechanics and flow environments in these two configurations. An asymmetric vortex system is observed downstream. The near-field is dom-

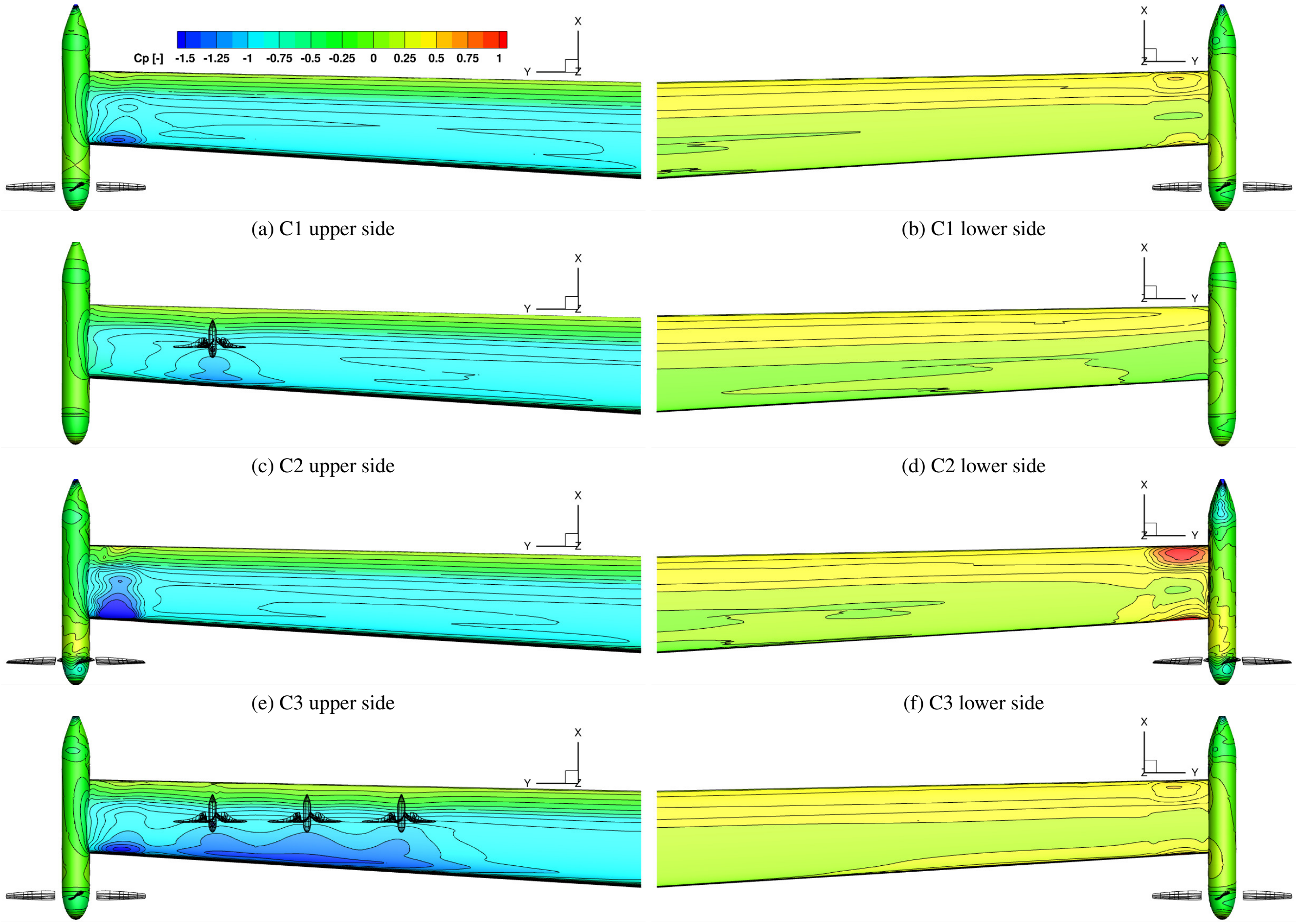

(a) C1 upper side (b) C1 lower side

(c) C2 upper side (d) C2 lower side

(e) C3 upper side (f) C3 lower side

(g) C4 upper side (h) C4 lower side

Figure 7. Averaged pressure coefficient from varies configurations.

inated by strong tip vortices and trailing edge vortices shed from the blade root with a higher twist. The nacelle vortex can also be differentiated across all cases, especially in the C3 configuration. Vortex shedding from the wing with the blunt trailing edge also interferes with the TMP. Two major differences can be identified when comparing these two configurations.

First, the C4 configuration has a reduced vorticity magnitude from the TMP and an earlier dissipation of the blade tip and root vortices. Slices [a] to [e] further show the paths of the wake, this suggests that the comparatively weaker wake from the TMP has a smaller impact on the wing. The vortices from the TMP in the C4 configuration indicate a higher degree of energy dissipation and tend to become more homogeneous propeller wakes than in the C3 configuration.

Second, the OTW installed DP system and their nacelles introduced additional vortices from the HLPs and their nacelles. Stronger vorticity can be seen in the DP system since it has a higher tip speed compared to the TMP system. The strength of the blade tip vortices is also reduced between the adjacent propellers due to the counter-rotating vortex system.

The thrust generated by the installed propellers varies across different configurations and conditions. Figure 9 presents an analysis of thrust distribution for all four configurations. The propellers exhibit asymmetric loads in all investigated cases, with variations depending on the configuration and operating conditions.

Figure 9(a) shows the thrust generated by the C1 propeller at different azimuth angles. It reveals that the TMP produces less thrust between azimuth angles of 0° and 90°, likely due to the higher induced velocity region created by the tip-mounted installation. Similarly, Figure 9(c) demonstrates a expanded reduction in thrust for the TMP between azimuth angles of 0° and 135°. This reduction is attributed to adverse effects caused by propeller-wing interactions at higher RPM conditions.

In the C4 configuration, Figure 9(d) indicates asymmetric thrust due to installation effects. Performance loss is observed when the HLP is positioned close to the wing between azimuth angles of 288° and 72°. Comparing the single installed HLP in Figure 9(b) with the distributed HLPs in Figure 9(d), the HLP adjacent to the TMP experiences a thrust loss between azimuth angles of 72° and 216°, indicating that the cooperative effect increase the induced velocity in those region and slightly reduce the propeller performance in those azimuth. Around 0°, the HLPs also shows slight unloading

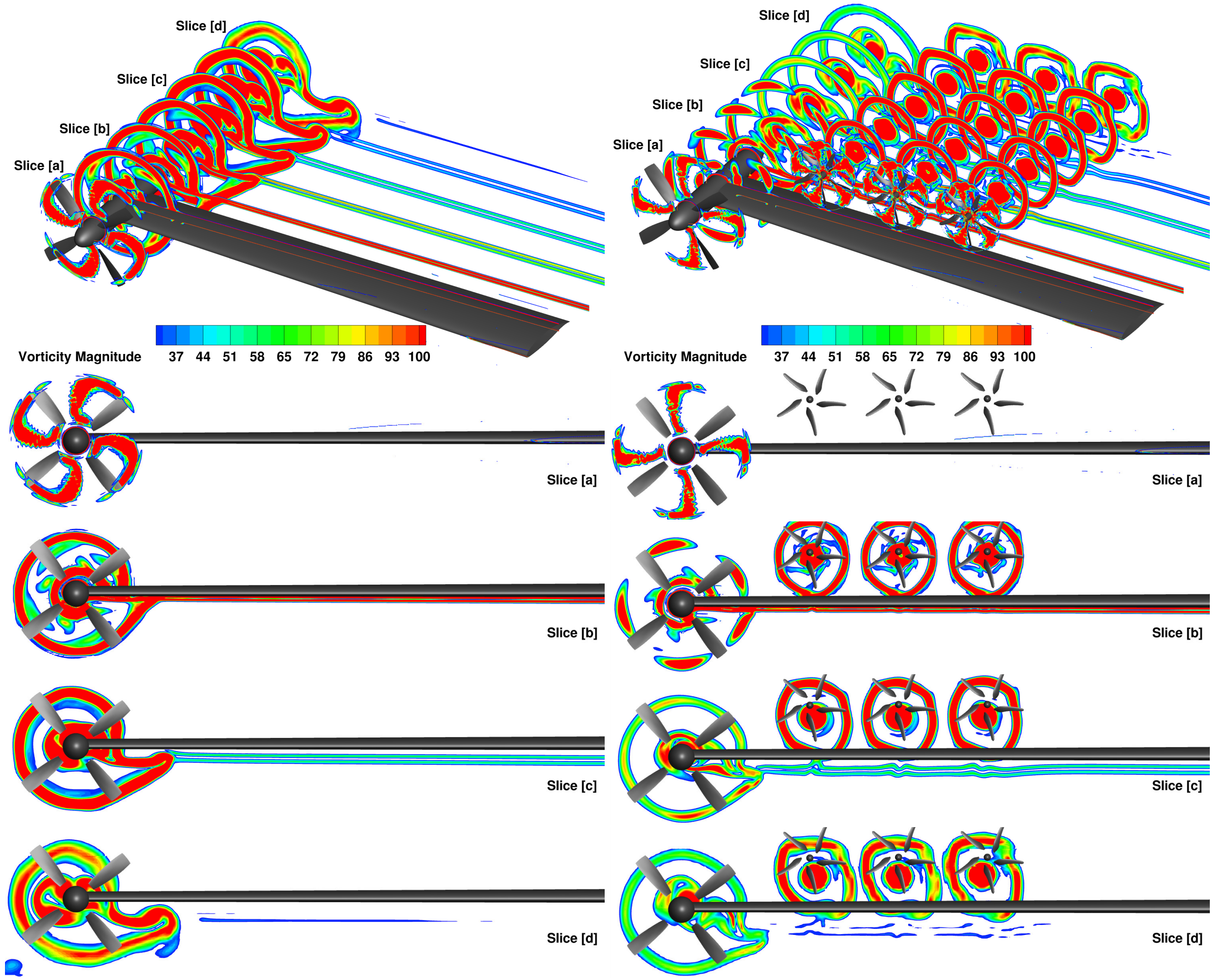

Figure 8. vortex distribution from varies configurations.

due to interactions with the TMP, wing and other HLPs.

Compared to the other two installed HLPs, the azimuths with higher thrust loads shift in a clockwise direction, while those experiencing performance loss tend to recover due to varying interaction mechanisms. This shift is attributed to the fact that the inboard propeller interacts primarily with the adjacent propeller and wing. Additionally, the increased wing chord length may lead to different levels of boundary layer ingestion.

The performance of individual components and the overall system for all configurations is presented in Figure 11. The TMPDP configuration exhibits the highest lift among the configurations studied. Variations in thrust for the tip-mounted propellers have a lesser impact on the lift and drag of the wing, resulting in only minor changes in the lift-to-drag ratio (L/D). The addition of the over-the-wing (OTW) distributed propulsion system significantly increases the nose-down pitching moment, as indicated in Table 2.

Comparing thrust-trimmed data between the TMP-only and TMPDP systems in the C3 and C4 configurations, the installed propellers generate similar thrust levels. The overall propeller efficiency is comparable between these two configurations, with the exception of the C1 configuration, where the TMP demonstrates superior efficiency at lower advance ratios.

Crucially, the data indicate that increasing the thrust setting in the TMP-only configuration enhances the overall propulsive efficiency. The introduction of the OTW-DP system was further beneficial to the overall efficiency, approaching nearly 60%, with a substantial improvement in wing lift generation. As a result, the integrated TMPDP system performs better than the other configurations.

CONCLUSIONS

In advanced propulsion system design for flying vehicles, existing configurations must be rethought due to the increased flexibility offered by hybrid/electric powertrain systems. This shift suggests an emergent need for knowledge, particularly

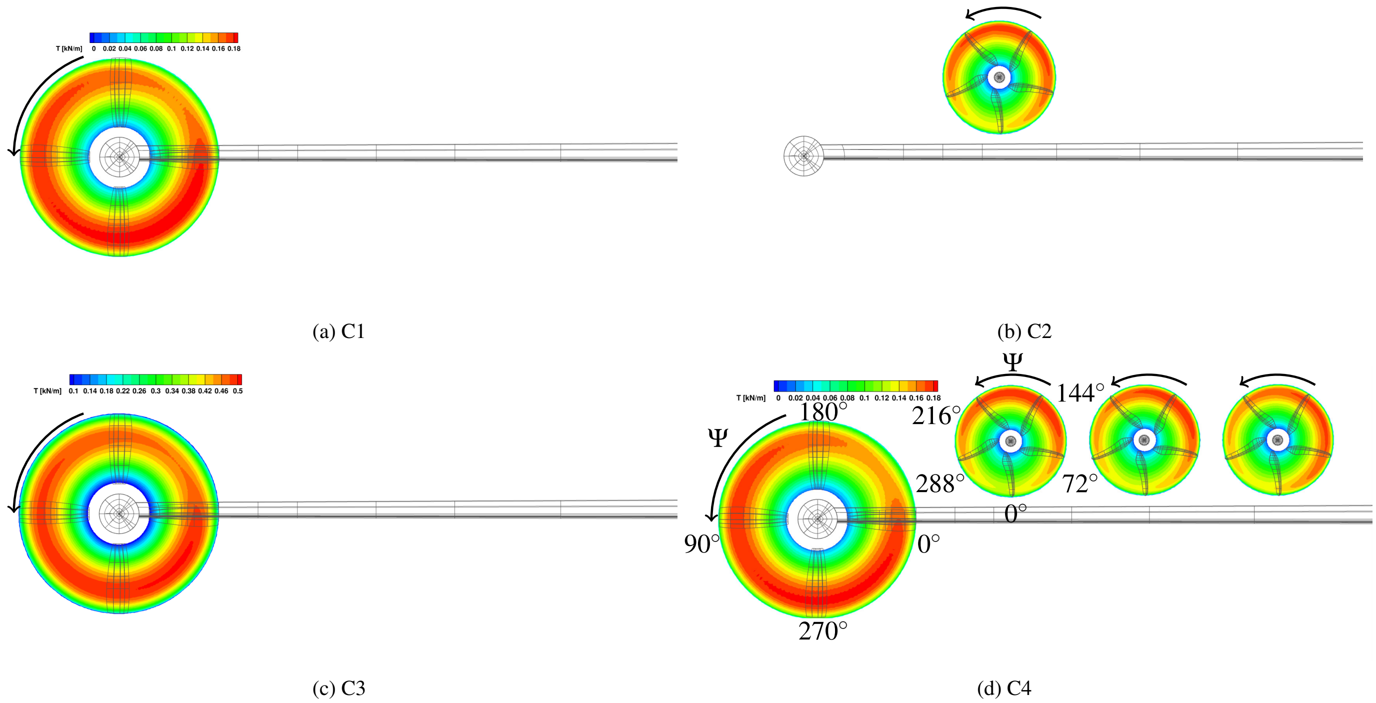

(a) C1

(b) C2

(c) C3

(d) C4

Figure 9. Propeller thrust distribution from varies configurations. (Rotation in counter-clockwise as seen from upstream)

Table 2. Summary of the performance of wing-only, Propeller-only, TMP and TMP-DP systems. (TMP1 is RPM matched in the TMP-DP case and TMP2 is thrust equivalent case, which matched to the Tecnam P2006T can have 52.6 kg thrust from semi-wing to achiveve T/W 0.149)

Performance	**C1**	**C2**	**C3**	**C4**	**Δ**
Proplellers performance:					
Thrust (N)	177.3	120	511.56	529.7 (174.52/118.8/118.0/118.4)	+3.5%
Power (kW)	6.53	5.5	22.35	22.82 (6.416/5.47/5.46/5.48)	+2.1%
Propeller Froude efficiency (-)	0.75	0.60	0.63	0.633 (0.748/0.596/0.593/0.594)	+0.5%
Pitching moment (Nm)	6.42	-46.3	15.41	-130.43 (6.52/-45.94/-45.72/-45.29)	
Wing performance:					
Lift (N)	958	901	987	1138	+15.3%
L/D (-)	14.45	14.6	14.6	27.6	+89.0%
Pitching moment (Nm)	-229.7	-219.7	-236.6	-248.5	
Overall efficiency (-)	46.8%	29.2%	54.6%	58.9%	+7.9%

regarding aero-propulsive synergistic effects. This study presents four propulsion systems using state-of-the-art modeling approaches, each aimed at enhancing performance. Current work covers aerodynamic performance, interaction effects, and configuration design in detail. The results demonstrate that the novel propulsion systems proposed can significantly improve overall propulsive efficiency and lift generation.

1. The study found that the placement of tip-mounted and distributed propulsion systems created an aerodynamic interference region with the wing. In the higher tip-speed case from configuration C3, this interference was more intense, reducing suction pressure near the leading edge and mid-chord region while increasing pressure at the leading and trailing edges on the pressure side due to wake-washing effects. The propeller-wing interaction caused thrust fluctuations as the propeller blades swept through the interference region, though the mean thrust was only slightly impacted, particularly in the lower tip-speed case from configuration C1.

2. Similar benefits, such as reduced suction pressure from the wing blow technique, were observed in the over-the-wing (OTW) installed high-lift propeller (HLP) in configuration C2. This benefit was even more pronounced in the distributed propulsion system of configuration C4, likely due to the cooperative effect. In the proposed TMP-DP configuration, no significant thrust loss was observed when transitioning from single to distributed pro-

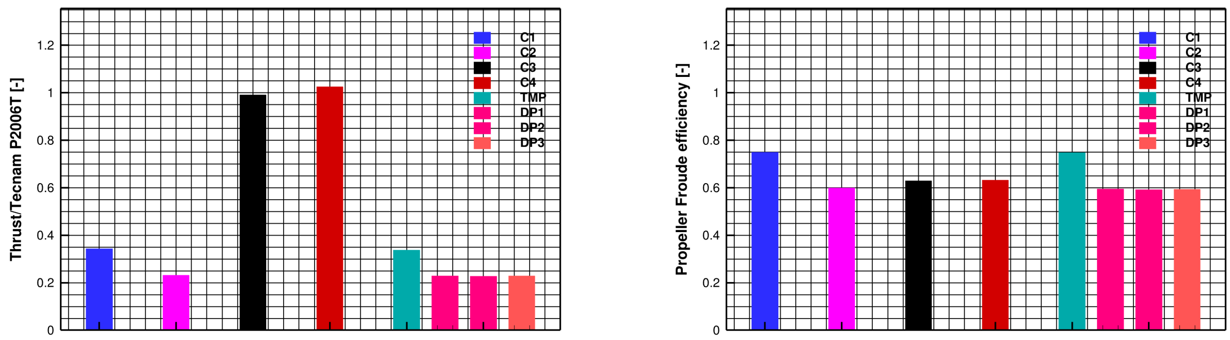

(a) Thrust ratio.

(b) propeller efficiency.

Figure 10. Comparisons of the thrust and propeller efficiency from various configurations.

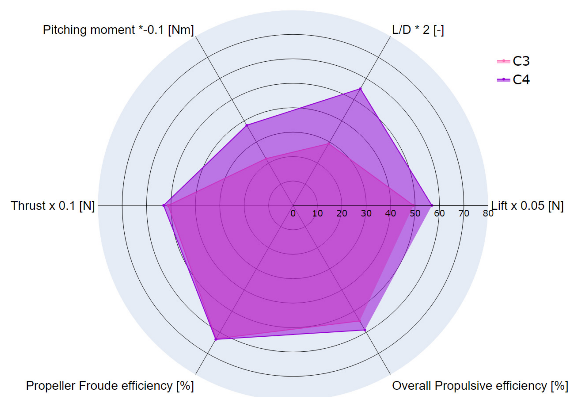

Figure 11. Comparisons of the TMP-only, OTW HLP installed, and equivalent performance of TMP and TMP-DP systems.

pellers. However, the TMP in configuration C4 exhibited thrust fluctuations similar to those in C1, indicating that TMP-DP-wing interactions have minimal impact on propeller performance within the TMP and DP systems.

3. The propellers within the DP system experienced similar sinusoidal variations in thrust, with the collective output of the TMP and three OTW propellers resulting in greater overall thrust fluctuations compared to the C3 configuration. The lift force distribution along the wingspan revealed a significant spike near the wingtip in the C3 configuration, which was substantially reduced in the C4 configuration. The increased lift generation near the most inboard OTW propeller may be attributed to the increased wing chord length. For the propellers, the TMP with higher RPM experience expanded thrust loss due to the installation, hence a better efficiency with lower RMP case. The installation of the DP system caused a slight reduction in the thrust of the TMP while passing through the wing suction side. At the same time, the cooperative effect of the DP slightly reduces the propeller performance while the propeller passes the wing and the adjacent propellers. However, the wing performance is much improved.

4. The structure of the vortex system in all configurations is affected by interactional effects, resulting in an asymmetric vortex system. In the TMP-only configuration, which provides equivalent propulsion force, the vortex generated is significantly stronger. The main deformed vortex tends to rise upward and propagate downstream and inboard. In configuration C4, there is a more rapid destruction of tip vortices and faster turbulent wake dissipation observed behind the TMP. The vortex system in the DP configuration introduces additional interference to the wing system. This interference deforms both the wake from the HLPs and the wing, with the middle HLPs exhibiting enhanced wake dissipation.

5. In terms of performance, configuration C4 generated 3.5% more thrust with improved efficiency. The enhanced wing performance resulted in nearly 15% more lift, and the overall efficiency gained 8%. The pitching moment was also analysed, while the wing produced a similar pitching moment between C3 and C4, the DP system in C4 contributed to a significantly higher pitching moment. This indicates that a new aerodynamic center

must be established to balance the aircraft when integrating a TMP-DP system into the full vehicle.

Author contact: Geng Qiao G.Qiao.1@research.gla.ac.uk George N. Barakos George.Barakos@glasgow.ac.uk

ACKNOWLEDGMENTS

The use of the EPSRC-funded ARCHIE-WeSt High-Performance Computer (www.archie-west.ac.uk) is gratefully acknowledged. Support via Greener Aviation with Advanced Propulsion Systems (GAAPS) EP/W010119/1 is gratefully acknowledged.

REFERENCES

1. Hermetz, J., Ridel, M., and Doll, C., "Distributed electric propulsion for small business aircraft a concept-plane for key-technologies investigations." *ICAS 2016, Sep 2016, DAEJEON, South Korea*, 2016.

2. Kim, H. D., Perry, A. T., and Ansell, P. J., "Progress in Distributed Electric Propulsion Vehicles and Technologies," Tech. rep., AIAA, 2020.

3. Patterson, M. D. and Borer, N. K., "Approach considerations in aircraft with high-lift propeller systems," *17th AIAA Aviation Technology, Integration, and Operations Conference*, 2017, p. 3782.

4. Stokkermans, T. C., Van Arnhem, N., Sinnige, T., and Veldhuis, L. L., "Validation and comparison of RANS propeller modeling methods for tip-mounted applications," *AIAA Journal*, Vol. 57, No. 2, 2019, pp. 566–580.

5. Loth, J. and Loth, F., "Induced drag reduction with wing tip mounted propellers," *2nd Applied Aerodynamics Conference*, 1984, p. 2149.

6. Miranda, L. and Brennan, J., "Aerodynamic effects of wingtip-mounted propellers and turbines," *4th Applied Aerodynamics Conference*, 1986, p. 1802.

7. PATTERSON, JR, J. and Bartlett, G., "Effect of a wing-tip mounted pusher turboprop on the aerodynamic characteristics of a semi-span wing," *21st Joint Propulsion Conference*, 1985, p. 1286.

8. Janus, J. M., Chatterjee, A., and Cave, C., "Computational analysis of a wingtip-mounted pusher turboprop," *Journal of aircraft*, Vol. 33, No. 2, 1996, pp. 441–444.

9. Heeg, J., Stanford, B. K., Kreshock, A., Shen, J., Hoover, C. B., and Truax, R., "Whirl Flutter and the Development of the NASA X-57 Maxwell," *International Forum on Aeroelasticity and Structural Dynamics (IFASD 2019)*, No. NF1676L-31615, 2019.

10. Borer, N. K., Patterson, M. D., Viken, J. K., Moore, M. D., Bevirt, J., Stoll, A. M., and Gibson, A. R., "Design and performance of the NASA SCEPTOR distributed electric propulsion flight demonstrator," *16th AIAA Aviation Technology, Integration, and Operations Conference*, 2016, p. 3920.

11. Hooker, J. R., Wick, A., Ginn, S. R., Walker, J., and Schiltgen, B. T., "Overview of Low Speed Wind Tunnel Testing Conducted on a Wingtip Mounted Propeller for the Workshop for Integrated Propeller Prediction," *AIAA AVIATION 2020 FORUM*, 2020, p. 2673.

12. Qiao, G., Zhang, T., and Barakos, G., "Numerical simulation of distributed propulsion systems using CFD," *Aerospace Science and Technology*, 2024, pp. 109011.

13. Steijl, R., Barakos, G., and Badcock, K., "A framework for CFD analysis of helicopter rotors in hover and forward flight," *International journal for numerical methods in fluids*, Vol. 51, No. 8, 2006, pp. 819–847, DOI: 10.1002/fld.1086.

14. Biava, M., Woodgate, M., and Barakos, G. N., "Fully implicit discrete-adjoint methods for rotorcraft applications," *AIAA Journal*, Vol. 54, No. 2, 2016, pp. 735–749, 10.2514/1.J054006.

15. Antoniadis, A., Drikakis, D., Zhong, B., Barakos, G., Steijl, R., Biava, M., Vigevano, L., Brocklehurst, A., Boelens, O., Dietz, M., et al., "Assessment of CFD methods against experimental flow measurements for helicopter flows," *Aerospace Science and Technology*, Vol. 19, No. 1, 2012, pp. 86–100, DOI: 10.1016/j.ast.2011.09.003.

16. Steijl, R. and Barakos, G., "CFD analysis of complete helicopter configurations–lessons learnt from the GOAHEAD project," *Aerospace Science and Technology*, Vol. 19, No. 1, 2012, pp. 58–71, DOI: 10.1016/j.ast.2011.01.007.

17. Han, D., Pastrikakis, V., and Barakos, G. N., "Helicopter flight performance improvement by dynamic blade twist," *Aerospace Science and Technology*, Vol. 58, 2016, pp. 445–452, DOI: 10.1016/j.ast.2016.09.013.

18. Garcia, A. J. and Barakos, G. N., "Numerical simulations on the ERICA tiltrotor," *Aerospace Science and Technology*, Vol. 64, 2017, pp. 171–191, 10.2514/6.2016-0329.

19. Dehaeze, F. and Barakos, G., "Mesh deformation method for rotor flows," *Journal of Aircraft*, Vol. 49, No. 1, 2012, pp. 82–92, DOI: 10.2514/1.C031251.

20. Chirico, G., Barakos, G., and Bown, N., "Numerical aeroacoustic analysis of propeller designs," *The Aeronautical Journal*, Vol. 122, No. 1248, 2018, pp. 283–315, DOI: 10.1017/aer.2017.123.

21. Crozon, C., Steijl, R., and Barakos, G., "Coupled flight dynamics and CFD - demonstration for helicopters in shipborne environment," *The Aeronautical Journal*, Vol. 122, No. 1247, 2018, pp. 42–82, DOI: 10.1017/aer.2017.112.

22. Babu, S., Loupy, G., Dehaeze, F., Barakos, G., and Taylor, N., "Aeroelastic simulations of stores in weapon bays using Detached-Eddy Simulation," *Journal of Fluids and Structures*, Vol. 66, October 2016, pp. 207–228, DOI: 10.1016/j.jfluidstructs.2016.07.014.

23. Barakos, G. and Johnson, C., "Acoustic comparison of propellers," *International Journal of Aeroacoustics*, Vol. 15, No. 6-7, 2016, pp. 575–594, DOI: 10.1177/1475472X16659214.

24. Higgins, R., Jimenez-Garcia, A., Barakos, G., and Bown, N., "High-Fidelity Computational Fluid Dynamics Methods for the Simulation of Propeller Stall Flutter," *AIAA Journal*, Vol. 57, No. 12, 2019, DOI: 10.2514/1.J058463.

25. Higgins, R., Barakos, G., and Jinks, E., "Estimation of Three-Dimensional Aerodynamic Damping using CFD," *The Aeronautical Journal*, Vol. 124, No. 1271, 2020, DOI: 10.1017/aer.2019.135.

26. Higgins, R., Zarev, A., Barakos, G., and Green, R., "Numerical Investigation of a Two-Bladed Propeller Inflow at Yaw," *Journal of Aircraft*, Vol. 57, No. 2, 2020, DOI: 10.2514/1.C035647.

27. Higgins, R., Barakos, G., Shahpar, S., and Tristanto, I., "An Aeroacoustic Investigation of a Tiltwing eVTOL Concept Aircraft," *AIAA Aviation 2020 Forum*, AIAA, 2020, DOI: 10.2514/6.2020-2684.

28. Zhang, T., Qiao, G., Smith, D., Barakos, G., and Kusyumov, A., "Parametric study of aerodynamic performance of equivalent ducted/un-ducted rotors," *Aerospace Science and Technology*, Vol. 117, 2021, pp. 106984, DOI: 10.1016/j.ast.2021.106984.

29. Qiao, G., *Parametric study of aerodynamic performance of equivalent ducted/un-ducted propellers based on high-fidelity computational fluid dynamics*, Master's thesis, University of Glasgow, 2021, http://theses.gla.ac.uk/id/eprint/82702.

30. Menter, F. R., "Two-equation eddy-viscosity turbulence models for engineering applications," *AIAA journal*, Vol. 32, No. 8, 1994, pp. 1598–1605, 10.2514/3.12149.

31. Qiao, G. and Barakos, G. N., "Verification and Optimisation of Distributed Propulsion Using High-Fidelity CFD Method," *American Helicopter Society 79th Annual Forum & Technology Display, May 16-18, 2023, West Palm Beach, Florida, USA*, 2023.

32. Qiao, G., Higgins, R. J., Barakos, G. N., and Zhang, T., "CFD Study of eVTOL Distributed Propulsors," *RAeS Applied Aerodynamics Conferencei, No.4 Hamilton Place, London, UK*, 13-15 September 2022, https://eprints.gla.ac.uk/280193/.

33. Biava, M. and Barakos, G. N., "Optimisation of ducted propellers for hybrid air vehicles using high-fidelity CFD," *The Aeronautical Journal*, Vol. 120, No. 1232, 2016, pp. 1632–1657, DOI: 10.1017/aer.2016.78.

34. Litherland, B. L., Borer, N. K., and Zawodny, N. S., "X-57 Maxwell High-Lift Propeller Testing and Model Development," *AIAA Aviation 2021 Forum, Virtual Event, August 2-6, 2021*, 2021, p. 3193, 10.2514/6.2021-3193.

35. Helden Aerospace, L. and Empirical Systems Aerospace, I., "Wind Tunnel Tesrting of Propeller Wingtip Interactions: Final wind tunnel test and CFD report for the Low Speed Wind Tunnel test of a 40.5% scale semi-span model with a wingtip-mounted propeller in the Lockheed Martin Low Speed Wind Tunnel," Tech. rep., Helden Aerospace, LLC. and Empirical Systems Aerospace, Inc., 2019.

36. Yin, J., De Gregorio, F., Rossignol, K.-S., Rottmann, L., Ceglia, G., Reboul, G., Barakos, G., Qiao, G., Muth, M., Kessler, M., Visingardi, A., Barbarino, M., Petrosino, F., Zanotti, A., Oberti, N., Galimberti, L., Bernardini, G., Poggi, C., Abergo, L., Caccia, F., Guardone, A., Testa, C., and Zaghi, S., "Acoustic and Aerodynamic Evaluation of DLR Small-Scale Rotor Configurations within GARTEUR AG26," *49th European Rotorcraft Forum (ERF), paper 80, Bückeburg, Germany*, September 5 – 7, 2023.